

# Spatial and Angular Resolution Enhancement of Light Fields Using Convolutional Neural Networks

M. Shahzeb Khan Gul and Bahadır K. Gunturk

Dept. of Electrical and Electronics Engineering, Istanbul Medipol University, Istanbul, Turkey  
mshkhangul@st.medipol.edu.tr bkgunturk@medipol.edu.tr

**Abstract**—Light field imaging extends the traditional photography by capturing both spatial and angular distribution of light, which enables new capabilities, including post-capture refocusing, post-capture aperture control, and depth estimation from a single shot. Micro-lens array (MLA) based light field cameras offer a cost-effective approach to capture light field. A major drawback of MLA based light field cameras is low spatial resolution, which is due to the fact that a single image sensor is shared to capture both spatial and angular information. In this paper, we present a learning based light field enhancement approach. Both spatial and angular resolution of captured light field is enhanced using convolutional neural networks. The proposed method is tested with real light field data captured with a Lytro light field camera, clearly demonstrating spatial and angular resolution improvement.

**Index Terms**—Light field, super-resolution, convolutional neural network.

## I. INTRODUCTION

Light field refers to the collection of light rays in 3D space. With a light field imaging system, light rays in different directions are recorded separately, unlike a traditional imaging system, where a pixel records the total amount of light received by the lens regardless of the direction. The angular light information enables new capabilities, including depth estimation, post-capture refocusing, post-capture aperture size and shape control, and 3D modelling. Light field imaging can be used in different application areas, including 3D optical inspection, robotics, microscopy, photography, and computer graphics.

Light field imaging is first described by Lippmann, who proposed to use a set of small biconvex lenses to capture light rays in different directions and refers to it as integral imaging [1]. The term "light field" was first used by Gershun, who studied the radiometric properties of light in space [2]. Adelson and Bergen used the term "plenoptic function" and defined it as the function of light rays at every possible location in space, going at every possible angle, for every wavelength, and at every time [3]. Adelson and Wang described and implemented a light field camera that incorporates a single main lens along with a microlens array [4]. This design approach is later adopted in commercial light field cameras [5], [6]. In 1996, Levoy and Hanrahan [7] and Gortler et al. [8] formulated light field as a 4D function, and studied ray space representation and light field re-sampling. Over the years, light field imaging theory and applications have continued to be developed further. Key developments include post-capture

refocusing [9], Fourier-domain light field processing [10], light field microscopy [11], focused plenoptic camera [12], and multi-focus plenoptic camera [13].

Light field acquisition can be done in various ways, such as camera arrays [14], optical masks [15], angle-sensitive pixels [16], and micro-lens arrays [10], [12]. Among these different approaches, micro-lens array (MLA) based light field cameras provide a cost-effective solution, and have been successfully commercialized [5], [6]. There are two basic implementation approaches of MLA-based light field cameras. In one approach, the image sensor is placed at the focal distance of the micro-lenses [10], [5]. In the other approach, a micro-lens relays the image (formed by the objective lens on an intermediate image plane) to the image sensor [12], [6].

In MLA-based light field cameras, there is a trade-off between spatial resolution and angular resolution since a single image sensor is used to capture both. For example, in the first generation Lytro camera, an 11 megapixel image sensor produces an 11x11 sub-aperture perspective images, each with a spatial resolution of about 0.1 megapixels. Such a low spatial resolution prevents the wide spread adoption of light field cameras. In recent years, different methods have been proposed to tackle the low spatial resolution issue. Hybrid systems, consisting of a light field sensor and a regular sensor, have been presented [19], [20], [21], where the high spatial resolution image from the regular sensor is used directly if needed or transferred to light field sub-aperture (perspective) images. The disadvantages of hybrid systems include increased cost and larger camera dimensions. Another approach is to apply multi-frame super-resolution techniques to the sub-aperture images of a light field [24], [26]. It is also possible to apply learning-based super-resolution techniques to each sub-aperture image of a light field [27].

In this paper, we present a convolutional neural network based light field super-resolution method. The method has two sub-networks; one is trained to increase angular resolution, that is, to synthesize novel viewpoints (sub-aperture images); and the other is trained to increase spatial resolution of each sub-aperture image. We show that the proposed method provides significant increase in image quality, visually as well as quantitatively (in terms of PSNR and SSIM [23]) and improves depth estimation accuracy.

The paper is organized as follows. We present the related work in the literature in Section II. We explain the proposed method in Section III, present our experimental results in Section IV, and conclude our paper in Section V.



Fig. 1: Light field captured by a Lytro Illum camera. A zoomed-in region is overlaid to show the individual lenslet regions.

## II. RELATED WORK

One of the first approaches that would come to mind to enhance the spatial resolution of images captured with an MLA-based light field camera is to apply a multi-frame super-resolution image restoration technique on the perspective images obtained from the light field capture. The Bayesian super-resolution restoration framework has been so far used, with Lambertian and textual priors [24], Gaussian mixture models [25], and variational models [26].

Learning-based single-image super-resolution methods can also be adopted to address the low spatial resolution issue of light fields. In [27], a dictionary learning based super-resolution method is presented, demonstrating a clear improvement over standard interpolation techniques when converting raw light field capture into perspective images. Another learning based method is presented in [28], which incorporates deep convolutional neural networks for spatial and angular resolution enhancement of light fields. Alternative to spatial domain resolution enhancement approaches, frequency domain methods, utilizing signal sparsity and Fourier slice theorem, have also been presented [30], [29].

In contrast to single-sensor light field imaging systems, hybrid light field imaging system have also been introduced to improve spatial resolution. In the hybrid imaging system proposed by Boominathan *et al.* [19], a patch-based algorithm is used to super-resolve low-resolution light field views using high-resolution patches acquired from a standard high-resolution camera. There are several other hybrid imaging system presented [20], [31], [21], combining images from a standard camera and a light field camera. Among these, the work in [21] demonstrates a wide baseline hybrid stereo system in addition to spatial resolution enhancement, improving range and accuracy of depth estimation as well.

## III. LIGHT FIELD SUPER RESOLUTION USING CONVOLUTIONAL NEURAL NETWORK

In Figure 1, a light field captured by a micro-lens array based light field camera (Lytro Illum) is shown. When

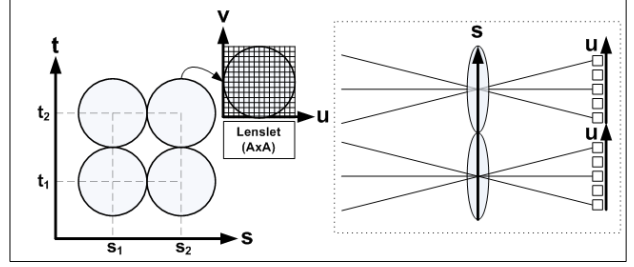


Fig. 2: Light field parameterization. Light field can be parameterized by the lenslet positions  $(s, t)$  and the pixel positions  $(u, v)$  behind a lenslet.

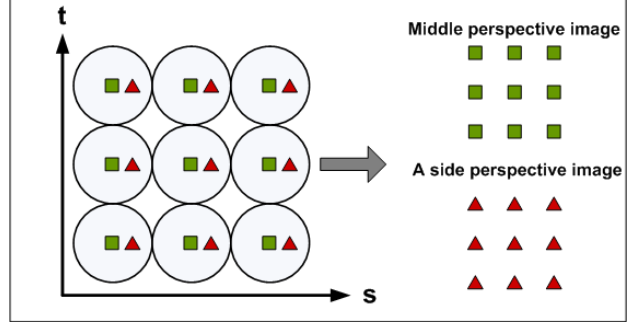


Fig. 3: Sub-aperture (perspective) image formation. A perspective image can be constructed by picking specific pixels from the lenslet regions. The size of a perspective image is determined by the number of lenslets.

zoomed-in, individual lenslet regions of the MLA can be seen. The pixels behind a lenslet region records directional light amounts received by that lenslet. As illustrated in Figure 2, it is possible to represent a light field with four parameters  $(s, t, u, v)$ , where  $(s, t)$  indicates the lenslet location, and  $(u, v)$  indicates the angular position behind the lenslet. A perspective image can be constructed by taking a single pixel value with a specific  $(u, v)$  index from each lenslet. The process is illustrated in Figure 3. The spatial resolution of a perspective image is controlled by the size and the number of the lenslets. Given a fixed image sensor size, the spatial resolution can be increased by having smaller size lenslets; given a fixed lenslet size, the spatial resolution can be increased by increasing the number of lenslets, thus, the size of the image sensor. The angular resolution, on the other hand, is defined by the number of pixels behind a lenslet region.

Our goal is to increase both spatial and angular resolution of a light field capture. We propose a deep learning method, which we call *deep light field super resolution* (DLFSR). It consists of two steps. Given a light field where there are  $A \times A$  pixels in each lenslet area and the size of each perspective is  $H \times W$ , the first step doubles the angular resolution from  $A \times A$  to  $2A \times 2A$  using a convolutional neural network. In the second step, the spatial resolution is doubled from  $H \times W$  to  $2H \times 2W$  by estimating new lenslet regions between given lenslet regions. Figure 4 gives an illustration of these steps.

The closest work in the literature to our method is the one presented in [28], which also uses deep convolutional

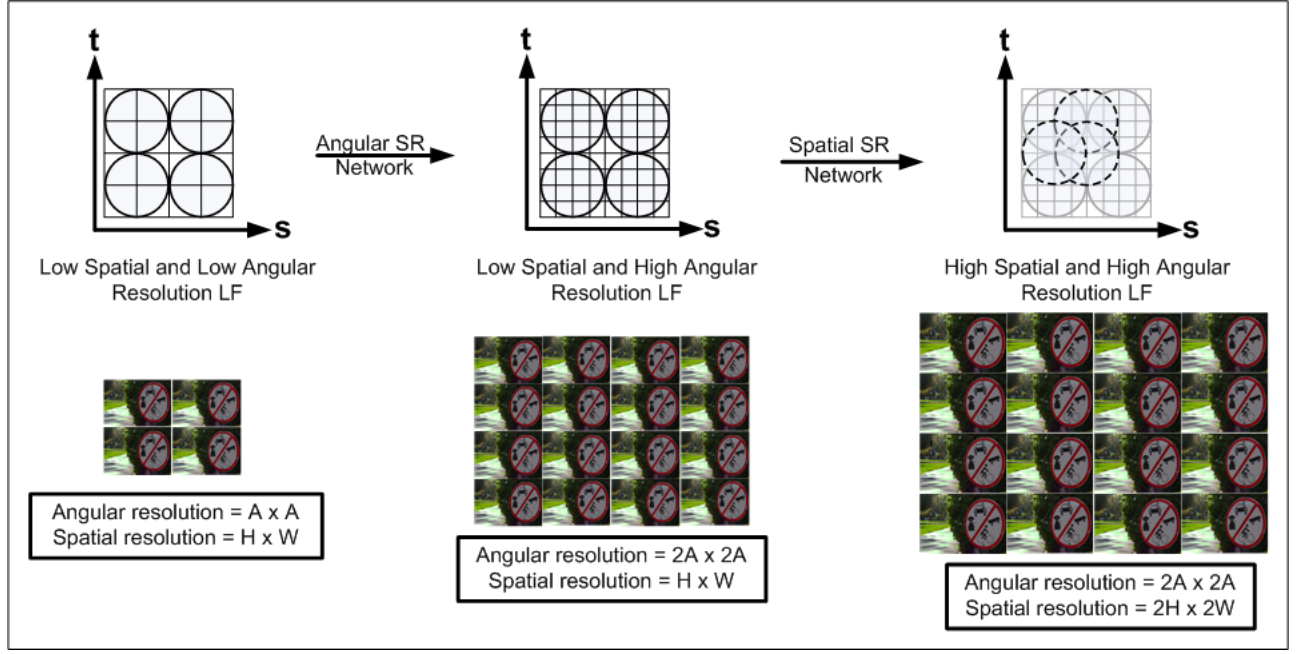


Fig. 4: An illustration of the proposed DLFSR method. First, the angular resolution is doubled; second, the spatial resolution is doubled. The networks are applied directly on the raw light field, not on the perspective images. The effect of each step on the perspective images is also illustrated.

networks. There is a fundamental difference between ours and the one in [28]; while our architecture is designed to work on raw light field data, that is, lenslet images; [28] is designed to work on perspective images. In the experimental results section, we provide both visual and quantitative comparison with [28].

#### A. Angular Super-Resolution (SR) Network

The proposed angular super-resolution network is shown in Figure 5. It is composed of two convolutional layers and a fully connected layer. The input to the network is a lenslet region with size  $A \times A$ ; and the output is a higher resolution lenslet region with size  $2A \times 2A$ . That is, the angular resolution enhancement is done directly on the raw light field (after demosaicking) as opposed to doing on perspective images. Each lenslet region is interpolated by applying the same network. Once the lenslet regions are interpolated, one can construct the perspective images by rearranging the pixels, as mentioned before. At the end,  $2A \times 2A$  perspective images are obtained from  $A \times A$  perspective images.

The convolution layers in the proposed architecture are based on the intuition that the first layer extracts a high-dimensional feature vector from the lenslet and the second convolutional layer maps it onto another high-dimensional vector. After each convolution layer, there is a non-linear activation layer of *Rectified Linear Unit* (ReLU). In the end, a fully connected layer aggregates the information of the last convolution layer and predicts a high-resolution version of the lenslet region.

The first convolution layer has  $n_1$  filters, each with size  $n_0 \times k_1 \times k_1$ . (In our experiments, we treat each color channel separately, thus  $n_0 = 1$ .) The second convolution layer has

$n_2$  filters, each with size  $n_1 \times k_2 \times k_2$ . The final layer is a fully connected layer with  $4A^2$  neurons, forming a  $2A \times 2A$  lenslet region.

#### B. Spatial Super-Resolution (SR) Network

Figure 6 gives an illustration of the spatial super-resolution network. Similar to the angular super-resolution network, the architecture has two convolutional layers, each followed by a ReLU layer, followed by a fully connected layer. Different from the angular resolution network, four lenslet regions are stacked together as the input to the network. There are three outputs at the end, predicting the horizontal, vertical, and diagonal sub-pixels of a perspective image. To clarify the idea further, Figure 7 illustrates the formation of a high-resolution perspective image. As mentioned earlier, a perspective image of a light field is formed by picking a specific pixel from each lenslet region and putting all picked pixels together. Using four lenslet regions, the network predicts three additional pixels in between the pixels picked from the lenslet regions. The predicted pixels, along with the picked pixels, form a higher resolution perspective image.

#### C. Training the Networks

We used a dataset that is captured by a Lytro Illum camera and is available online [32]. The dataset has more than 200 raw light fields, each with angular resolution of  $14 \times 14$  and spatial resolution of  $374 \times 540$ . In other words, each light field consists of  $14 \times 14$  perspective images; and each perspective image has spatial resolution of  $374 \times 540$  pixels. The raw light field is of size  $5236 \times 7560$ , consisting of  $374 \times 540$  lenslet regions, where each lenslet region has  $14 \times 14$  pixels. We used 45 light fields

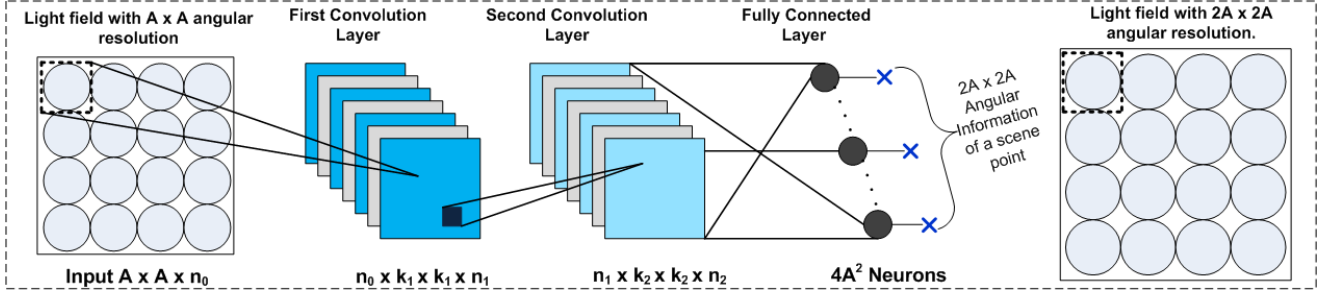


Fig. 5: Overview of the angular SR network to estimate a high angular resolution version of the input light field. A lenslet is drawn as a circle; the  $A \times A$  region behind a lenslet is taken as the input and processed to predict a  $2A \times 2A$  lenslet region. Each convolution layer is followed by a non-linear activation layer of ReLU.

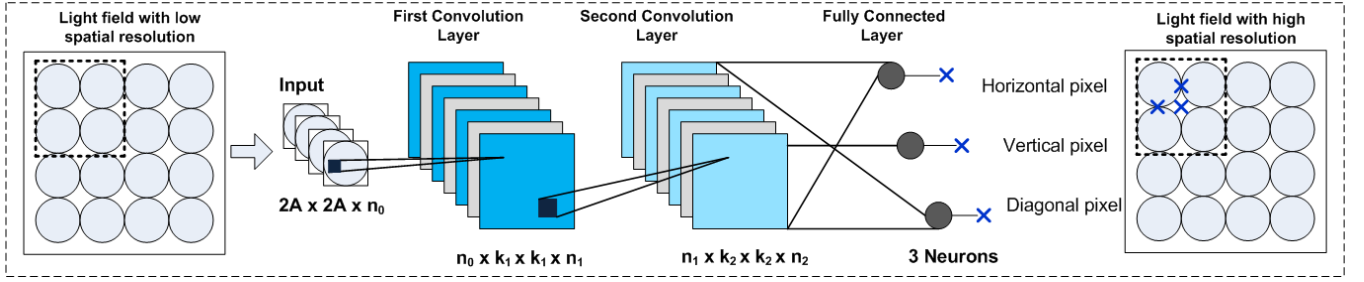


Fig. 6: Overview of the proposed spatial SR network to estimate a higher spatial resolution version of the input light field. Four lenslet regions are stacked and taken as the input to the network. The network predicts three new pixels to be used in high-resolution perspective image formation. Each convolution layer is followed by a non-linear activation layer of ReLU.

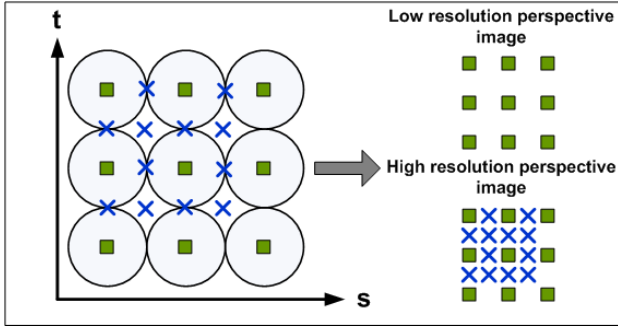


Fig. 7: Constructing a high-resolution perspective image. A perspective image can be formed by picking a specific pixel from each lenslet region, and putting all picked pixels together. Using the additional pixels predicted by the spatial SR network, a higher resolution perspective image is formed.

for training and reserved the others for testing. The training data is obtained in two steps. First, we drop every other lenslet region to obtain a low-spatial-resolution ( $187 \times 270$ ) and high-angular-resolution ( $14 \times 14$ ) light field. Second, we drop every other pixel in a lenslet region to obtain a low-spatial-resolution ( $187 \times 270$ ) and low-angular-resolution ( $7 \times 7$ ) light field.

The angular SR network, as shown in Figure 5, has low-spatial-resolution and low-angular-resolution light field as its input, and low-spatial-resolution and high-angular-resolution light field as its output. Each lenslet region is treated separately by the network, increasing the size from  $7 \times 7$  to  $14 \times 14$ . The first convolution layer consists of 64 filters, each with size

$3 \times 3$ . It is followed by a ReLU layer. The second convolution layer consists of 32 filters of size  $64 \times 1 \times 1$ , followed by a ReLU layer. Finally, there is a fully connected layer with 196 neurons at the end to produce a  $14 \times 14$  lenslet region.

The spatial super-resolution network, as shown in Figure 6, has low-spatial-resolution and high-angular-resolution light field as its input, and high-spatial-resolution and high-angular-resolution light field as its output. Four lenslet regions are stacked to form a  $14 \times 14 \times 4$  input. The first convolution layer consists of 64 filters, each with size  $4 \times 3 \times 3$ . The second convolution layer consists of 32 filters of size  $64 \times 1 \times 1$ . Each convolution layer is followed by a ReLU layer. Finally, there is a fully connected layer with three neurons at the end to produce the horizontal, vertical and diagonal pixels. This network generates one high-spatial resolution perspective. For each perspective, the network is trained separately.

We implement and train our model using the Caffe package [33]. For the weight initialization of both networks, we used Xavier's initialization technique [34], with mean set to zero and standard deviation set to  $10^{-3}$ , to prevent vanishment or over-amplification of weights. The learning rate for the three layers of the networks is  $10^{-3}$ ,  $10^{-3}$ , and  $10^{-5}$ , respectively. Mean squared error is used as the loss function, which is minimized using the stochastic gradient descent method with standard backpropagation [35]. For each network, the input size is about 13 million; and the number of iterations is almost  $10^7$ .



#### IV. EXPERIMENTS

We evaluated our DLFSR method on 25 test light fields, which we reserved from the Lytro Illum camera dataset [32]. We compared our results with the state-of-the-art convolutional neural network based light field super resolution method, called LFCNN [28]. We implemented the LFCNN networks using the parameters provided by the authors [28]. In addition to spatial resolution enhancement, we investigated depth estimation performance, and compared the depth maps generated by low-resolution light fields and the resolution-enhanced light fields.

##### A. Spatial Resolution Enhancement

The test images are downsampled from 14x14 perspective images, each with size 374x540 pixels, to 7x7 perspective images with size 187x270 pixels. The trained networks are applied to these low-spatial and -angular resolution images to bring them back to the original spatial and angular resolutions. The networks are applied on each color channel separately. Since the original perspective images are available, we can quantitatively calculate the performance by comparing the estimated and the original images. In Table I, we provide peak-signal-to-noise ratio (PSNR) and SSIM [23] results of our method, in addition to the results of the LFCNN [28] method and bicubic interpolation, which serves as a baseline. The proposed method has more than 2.8dB improvement over bicubic interpolation on average. The PSNR performance of LFCNN [28] is worse than the bicubic interpolation.

In Figures 8, 9 and 10, we provide visual comparisons. The proposed DLFSR generates sharper and visually pleasing images. In the visual evaluation, we notice that the LFCNN method produces sharper results compared to the bicubic interpolation, despite having lower PSNR and SSIM values. This is mainly due to the over-sharpening of the LFCNN method.

##### B. Depth Map Estimation Accuracy

One of the capabilities of light field imaging is depth map estimation, whose accuracy is directly related to the angular resolution of light field. In Figure 11, and 12, we compare depth maps obtained from the input light fields and the light fields enhanced by the proposed method. The depth maps are estimated using the method in [38], which is specifically designed for light fields. It is clearly visible that depth maps obtained from light fields enhanced with the proposed method show higher accuracy. With the enhanced light fields, even close depths can be differentiated, unlike the low-resolution light fields.

##### C. Further Increasing the Spatial Resolution

For quantitative evaluation, we need to have the ground truth; thus, we downsample the captured light field to generate its lower resolution version. We can also visually evaluate the performance of the proposed method without downsampling. In Figure 13, we provide a comparison of the bicubic interpolation, the LFCNN method, and the proposed method, when the

input is the original light field capture. The spatial resolution of each perspective image is increased from 374x540 to 748x1080. From the figure, it is seen that the performance of our method is again better than both bicubic interpolation and the LFCNN [28] method.

#### V. DISCUSSION AND CONCLUSIONS

In this paper, we presented a convolutional neural network based light field super-resolution method. The method consists of two separate deep convolution neural networks trained through supervised learning. The architecture of these networks are composed of only three layers, reducing computational complexity. The proposed method shows significant improvement both quantitatively and visually over the baseline bicubic interpolation and another deep learning based light field super resolution method. We also demonstrated that enhanced light field results in more accurate depth map estimation due to the increase in angular resolution.

The spatial super-resolution network is designed to generate one perspective image. One may suggest to generate all perspectives in a single run; however, this would result in a larger network, requiring larger size dataset and more training. Instead, we preferred to have a simple, specialized, and effective architecture.

Similar to other neural network based super-resolution techniques, the method is designed to increase the resolution by an integer factor (two). It can be applied multiple times to increase the resolution by factors of two. A non-integer factor size changes is also possible by first interpolating using the proposed method and then downsampling using a standard technique. This is a well-known approach, and it will not be investigated in this paper.

The network parameters are optimized for a specific light field camera. For different cameras, the specific network parameters, such as filter dimensions, may need to be optimized. We, however, believe that the overall architecture is generic and would work well with any light field imaging system, once optimized.

#### REFERENCES

- [1] G. Lippmann, "Epreuves reversibles, photographies integrales," *J. Academie des sciences*, pp. 446–451, 1908.
- [2] A. Gershun, "The light field," *J. of Mathematics and Physics*, vol. 18, 1936.
- [3] E. H. Adelson and J. R. Bergen, "The plenoptic function and the elements of early vision," *Vision and Modeling Group, Media Laboratory, Massachusetts Institute of Technology*, 1991.
- [4] E. H. Adelson and J. Wang, "Single lens stereo with a plenoptic camera," *IEEE Trans. on Pattern Analysis and Machine Intelligence*, vol. 14, no. 2, pp. 99–106, 1992.
- [5] "Lytro, inc." <https://www.lytro.com/>.
- [6] "Raytrix, gmbh." <https://www.raytrix.de/>.
- [7] M. Levoy and P. Hanrahan, "Light field rendering," in *Proc. of the 23rd Annual Conf. on Computer Graphics and Interactive Techniques*. ACM, 1996, pp. 31–42.
- [8] S. J. Gortler, R. Grzeszczuk, R. Szeliski, and M. F. Cohen, "The lumigraph," in *Proc. of the 23rd Annual Conf. on Computer Graphics and Interactive Techniques*. ACM, 1996, pp. 43–54.
- [9] A. Isaksen, L. McMillan, and S. J. Gortler, "Dynamically reparameterized light fields," in *Proc. of SIGGRAPH*, 2000, pp. 297–306.
- [10] R. Ng, "Fourier slice photography," in *ACM Trans. on Graphics (TOG)*, vol. 24, no. 3, 2005, pp. 735–744.

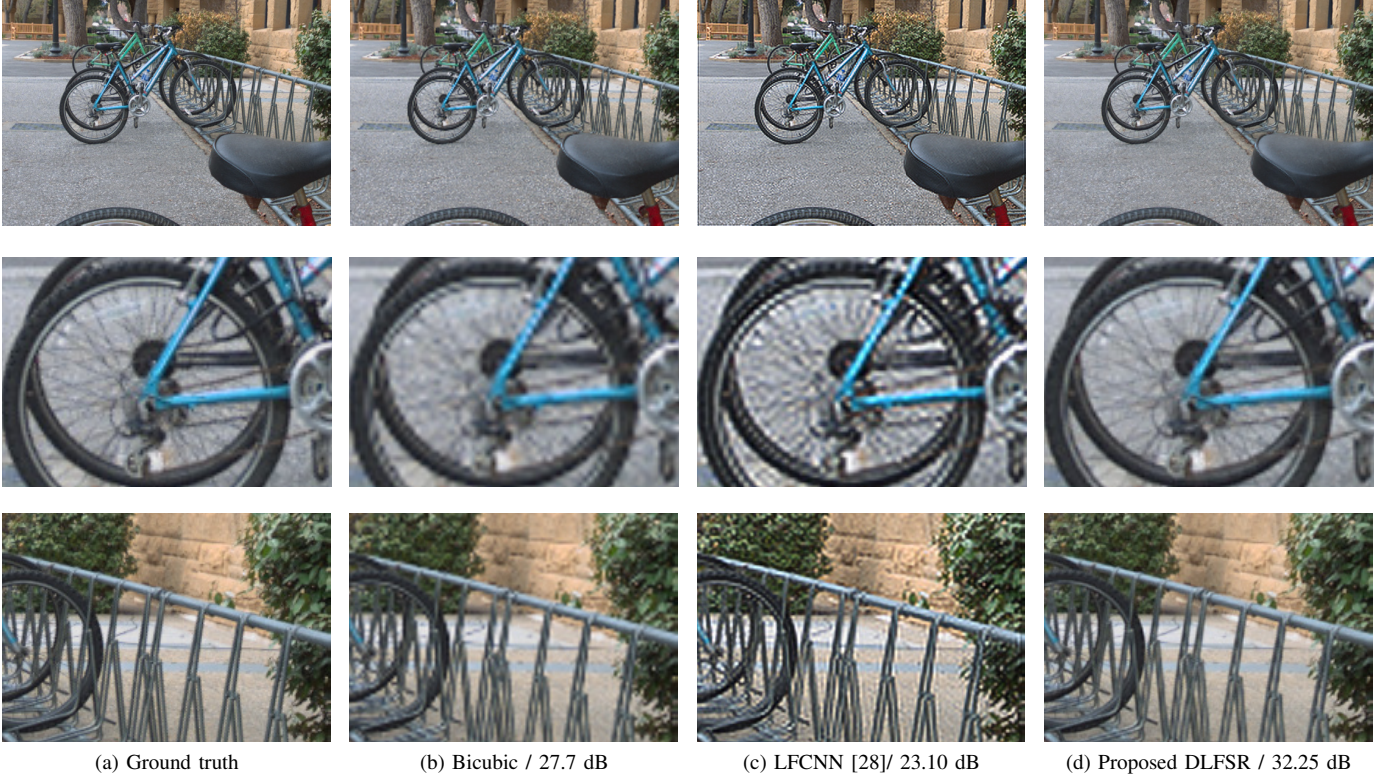


Fig. 8: Visual comparison of different methods. Middle perspective image is shown.



Fig. 9: Visual comparison of different methods. Middle perspective image is shown.



Methods	PSNR (dB)			SSIM		
	Min	Avg	Max	Min	Avg	Max
Bicubic	27.2620	30.6245	37.1640	0.578	0.9256	0.9659
LFCNN [28]	17.9591	21.7345	29.2083	0.7815	0.8590	0.9211
Proposed DLFSR	<b>29.7515</b>	<b>33.4273</b>	<b>39.5655</b>	<b>0.9360</b>	<b>0.9559</b>	<b>0.9823</b>

TABLE I: Quantitative comparison of different methods.



Fig. 10: Visual comparison of different methods. Middle perspective image is shown.

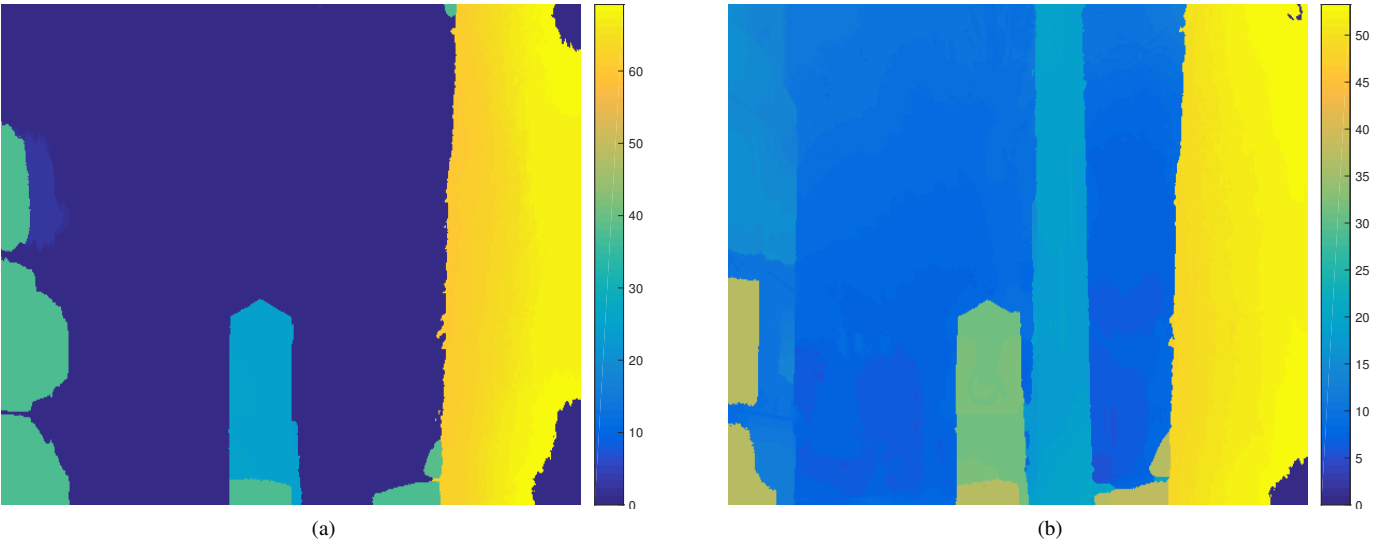


Fig. 11: Depth map estimation accuracy. The depth maps are generated for the image shown in Figure 9. (a) Estimated depth from the input light field with 7x7 angular resolution. (b) Estimated depth from enhanced light field of 14x14 angular resolution.

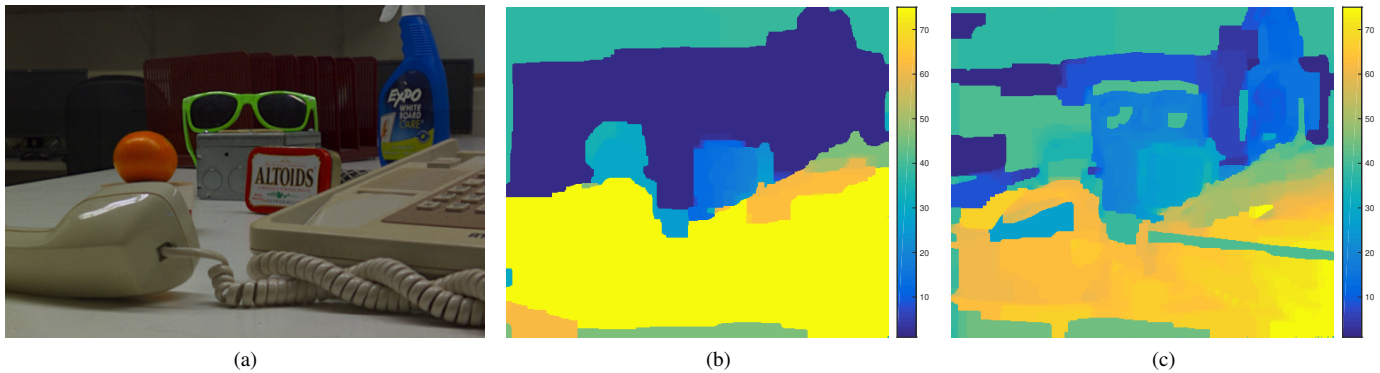
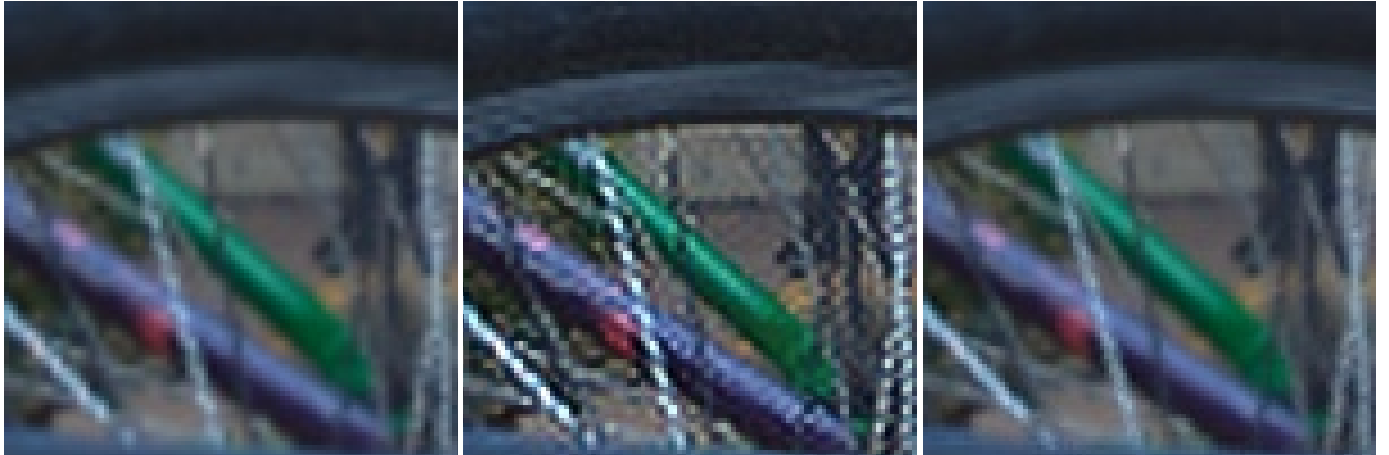


Fig. 12: Depth map estimation accuracy. (a) Middle perspective image. (b) Estimated depth from the input light field of  $7 \times 7$  angular resolution. (c) Estimated depth from enhanced light field with  $14 \times 14$  angular resolution.

- [11] M. Levoy, R. Ng, A. Adams, M. Footer, and M. Horowitz, "Light field microscopy," *ACM Trans. Graph.*, vol. 25, no. 3, pp. 924–934, 2006.
- [12] A. Lumsdaine and T. Georgiev, "The focused plenoptic camera," in *IEEE Int. Conf. on Computational Photography*, 2009, pp. 1–8.
- [13] C. Perwass and L. Wietzke, "Single lens 3D-camera with extended depth-of-field," in *Proc. SPIE Human Vision and Electronic Imaging*, 2012, p. 829108.
- [14] B. Wilburn, N. Joshi, V. Vaish, E.-V. Talvala, E. Antunez, A. Barth, A. Adams, M. Horowitz, and M. Levoy, "High performance imaging using large camera arrays," in *ACM Trans. on Graphics (TOG)*, vol. 24, no. 3, 2005, pp. 765–776.
- [15] A. Veeraraghavan, R. Raskar, A. Agrawal, A. Mohan, and J. Tumblin, "Dappled photography: Mask enhanced cameras for heterodyned light fields and coded aperture refocusing," *ACM Trans. on Graphics (TOG)*, vol. 26, no. 3, p. 69, 2007.
- [16] A. Wang, P. R. Gill, and A. Molnar, "An angle-sensitive cmos imager for single-sensor 3d photography," in *IEEE Int. Solid-State Circuits Conference Digest of Technical Papers (ISSCC)*. IEEE, 2011, pp. 412–414.
- [17] K. I. Kim and Y. Kwon, "Single-image super-resolution using sparse regression and natural image prior," *IEEE Trans. on Pattern Analysis and Machine Intelligence*, vol. 32, no. 6, pp. 1127–1133, 2010.
- [18] J. Sun, Z. Xu, and H.-Y. Shum, "Image super-resolution using gradient profile prior," in *IEEE Conf. on Computer Vision and Pattern Recognition*, 2008, pp. 1–8.
- [19] V. Boominathan, K. Mitra, and A. Veeraraghavan, "Improving resolution and depth-of-field of light field cameras using a hybrid imaging system," in *IEEE Int. Conf. on Computational Photography*. IEEE, 2014, pp. 1–10.
- [20] X. Wang, L. Li, and G. Hou, "High-resolution light field reconstruction using a hybrid imaging system," *Applied Optics*, vol. 55, no. 10, pp. 2580–2593, 2016.
- [21] M. Z. Alam and B. K. Gunturk, "Hybrid stereo imaging including a light field and a regular camera," in *Signal Processing and Communication Application Conference (SIU)*. IEEE, 2016, pp. 1293–1296.
- [22] Z. Wang, D. Liu, J. Yang, W. Han, and T. Huang, "Deep networks for image super-resolution with sparse prior," in *Proceedings of the IEEE International Conference on Computer Vision*, 2015, pp. 370–378.
- [23] Z. Wang, A. C. Bovik, H. R. Sheikh, and E. P. Simoncelli, "Image quality assessment: from error visibility to structural similarity," *IEEE Transactions on image processing*, vol. 13, no. 4, pp. 600–612, 2004.
- [24] T. E. Bishop, S. Zanetti, and P. Favaro, "Light field superresolution," in *IEEE Int. Conf. on Computational Photography*, 2009, pp. 1–9.
- [25] K. Mitra and A. Veeraraghavan, "Light field denoising, light field superresolution and stereo camera based refocussing using a gmm light field patch prior," in *IEEE Computer Society Conf. on Computer Vision and Pattern Recognition Workshops*, 2012, pp. 22–28.
- [26] S. Wanner and B. Goldluecke, "Spatial and angular variational super-resolution of 4d light fields," in *European Conf. on Computer Vision*. Springer, 2012, pp. 608–621.
- [27] D. Cho, M. Lee, S. Kim, and Y.-W. Tai, "Modeling the calibration pipeline of the lytro camera for high quality light-field image reconstruction," in *Proc. of the IEEE Int. Conf. on Computer Vision*, 2013, pp. 3280–3287.
- [28] Y. Yoon, H.-G. Jeon, D. Yoo, J.-Y. Lee, and I. So Kweon, "Learning a deep convolutional network for light-field image super-resolution," in *Proc. of the IEEE Int. Conf. on Computer Vision Workshops*, 2015, pp. 24–32.
- [29] L. Shi, H. Hassanieh, A. Davis, D. Katabi, and F. Durand, "Light field reconstruction using sparsity in the continuous fourier domain," *ACM Trans. on Graphics (TOG)*, vol. 34, no. 1, p. 12, 2014.
- [30] F. Pérez, A. Pérez, M. Rodríguez, and E. Magdaleno, "Fourier slice super-resolution in plenoptic cameras," in *IEEE Int. Conf. on Computational Photography*. IEEE, 2012, pp. 1–11.
- [31] J. Wu, H. Wang, X. Wang, and Y. Zhang, "A novel light field super-resolution framework based on hybrid imaging system," in *Visual Communications and Image Processing (VCIP)*. IEEE, 2015, pp. 1–4.
- [32] A. S. Raj, M. Lowney, and R. Shah, "Light-field database creation and depth estimation," <https://lightfields.stanford.edu/>.
- [33] Y. Jia, E. Shelhamer, J. Donahue, S. Karayev, J. Long, R. Girshick, S. Guadarrama, and T. Darrell, "Caffe: Convolutional architecture for fast feature embedding," in *Proc. of the 22nd ACM Int. Conf. on Multimedia*, 2014, pp. 675–678.
- [34] X. Glorot and Y. Bengio, "Understanding the difficulty of training deep feedforward neural networks," in *Aistats*, vol. 9, 2010, pp. 249–256.
- [35] Y. LeCun, L. Bottou, Y. Bengio, and P. Haffner, "Gradient-based learning applied to document recognition," *Proceedings of the IEEE*, vol. 86, no. 11, pp. 2278–2324, 1998.
- [36] S. Wanner, S. Meister, and B. Goldluecke, "Datasets and benchmarks for densely sampled 4d light fields," in *VMV*, 2013, pp. 225–226.
- [37] Y. Yoon, H.-G. Jeon, D. Yoo, J.-Y. Lee, and I. S. Kweon, "Light-field image super-resolution using convolutional neural network," *IEEE Signal Processing Letters*, vol. 24, no. 6, pp. 848–852, 2017.
- [38] H.-G. Jeon, J. Park, G. Choe, J. Park, Y. Bok, Y.-W. Tai, and I. So Kweon, "Accurate depth map estimation from a lenslet light field camera," in *Proceedings of the IEEE Conference on Computer Vision and Pattern Recognition*, 2015, pp. 1547–1555.

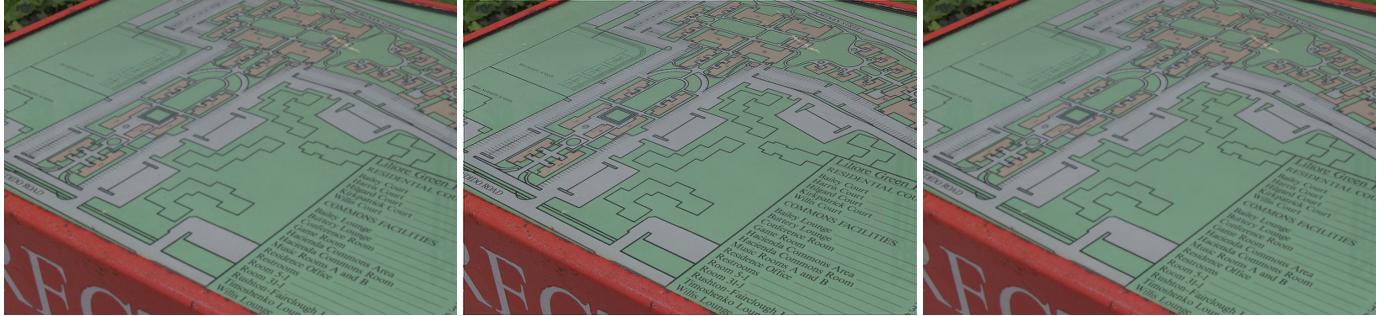




(a) Bicubic

(b) LFCNN [28]

(c) Proposed DLFSR



(d) Bicubic

(e) LFCNN [28]

(f) Proposed DLFSR

Fig. 13: Visual comparison of different methods. Middle perspective image is shown.